Bistatic SAR Image Formation and Interferometric Processing for the Stereoid Earth Explorer 10 Candidate Mission

Prats-Iraola, Pau; Pinheiro, Muriel; Rodriguez-Cassola, Marc; Scheiber, Rolf; Lopez-Dekker, Paco

DOI
10.1109/IGARSS.2019.8897930

Publication date
2019

Document Version
Accepted author manuscript

Published in
2019 IEEE International Geoscience and Remote Sensing Symposium, IGARSS 2019 - Proceedings

Citation (APA)
Prats-Iraola, P., Pinheiro, M., Rodriguez-Cassola, M., Scheiber, R., & Lopez-Dekker, P. (2019). Bistatic SAR Image Formation and Interferometric Processing for the Stereoid Earth Explorer 10 Candidate Mission. In *2019 IEEE International Geoscience and Remote Sensing Symposium, IGARSS 2019 - Proceedings* (pp. 106-109). Article 8897930 Institute of Electrical and Electronics Engineers (IEEE). https://doi.org/10.1109/IGARSS.2019.8897930

BISTATIC SAR IMAGE FORMATION AND INTERFEROMETRIC PROCESSING FOR THE STEREOID EARTH EXPLORER 10 CANDIDATE MISSION

Pau Prats-Iraola[a], Muriel Pinheiro[a], Marc Rodriguez-Cassola[a], Rolf Scheiber[a], Paco Lopez-Dekker[b]

[a] German Aerospace Center (DLR), Microwaves and Radar Institute, Germany

[b] Delft University of Technology, The Netherlands

ABSTRACT

This paper addresses the aspects of image formation and interferometric processing in the frame of the STEREOID Earth Explorer 10 candidate mission. In particular, the large along-track baseline configuration (approx. $250\ \mathrm{km}$), which results in a high Doppler centroid, will be addressed in terms of bistatic SAR image formation and interferometric processing. The proposed focusing algorithm is validated with point-target simulations, while the interferometric investigations are performed using raw data generated with a bistatic end-to-end simulator.

Index Terms**—** Synthetic Aperture Radar (SAR), interferometric SAR (InSAR), bistatic SAR, companion satellite

1. INTRODUCTION

The STEREOID (Stereo Thermo-optically Enhanced Radar for Earth, Ocean, Ice, and land Dynamics) mission concept has been selected as candidate mission for ESA's Earth Explorer 10. It consists of two identical small satellites carrying a receive-only radar instrument as main payload flying in a reconfigurable formation with Sentinel-1C or D, which will work as transmitter. The radar measurements are to be enhanced and supported by a medium resolution dual visible and near-infrared (VNIR) and thermal infrared (TIR) payload. The STEREOID mission will be organized in several phases, with different formation configurations optimized for the retrieval of deformation fields over land, ice, and oceans, and topography changes over land and ice, respectively. In all mission phases, the STEREOID-A and B satellites will be flying at an along-track distance of about $250\ \mathrm{km}$ to the transmitter.

The following sections analyze the technical aspects related to bistatic SAR image formation and InSAR processing under the presence of the large Doppler centroid due to the along-track baseline.

2. BISTATIC SAR IMAGE FORMATION

Monostatic SAR focusing is already a quite established topic and several efficient algorithms can be found in the literature [1]. In bistatic systems with platforms flying in close-formation (less than $20\ \mathrm{km}$) the acquisition geometry is quasi-monostatic, implying that the equivalent velocity approximation holds for moderate resolutions.

However, the equivalent velocity approximation becomes less accurate the larger the along-track baseline between transmitter and receiver. Fig. 1 shows a sketch of the STEREOID acquisition geometry with an along-track separation of $250\ \mathrm{km}$. The squint angle relevant for processing is depicted, where one needs to half it due to the bistatic operation. The bistatic squint angles go from approx. $-15°$ to $-13°$ at near and far range of the IW mode, respectively, with the corresponding Doppler centroids of about $-35\ \mathrm{kHz}$ and $-31\ \mathrm{kHz}$. The processing of bistatic data under large squints and large Doppler centroids is challenging due to the coupling between the range and azimuth signals, and enough literature exists to efficiently solve this problem for a *flat geometry*. But not only must the squint angle be considered, also the complete *spaceborne geometry* needs to be addressed. Indeed, Earth's rotation and the curved orbit introduce a non-hyperbolic range history. Therefore, similar to high resolution spaceborne SAR imaging [2, 3], the processor needs to properly account for it. Due to the non-hyperbolic range history, it is not possible to obtain a *compact* analytic expression of the point target spectrum, which would ideally be necessary in order to achieve proper focusing using Fourier-based kernels. For this reason a numerical approach has been selected in order to compute the kernel of the processor, similar as proposed in [4, 2, 5]. In addition, due to the large squint angle, monochromatic kernels do not achieve proper focusing. Indeed, deterioration for ranges other than the reference range occurs due to the limited performance of monochromatic kernels to accommodate the range dependency of the secondary range compression (SRC) and higher order terms.

Instead of trying to patch up a monochromatic kernel to achieve focusing (e.g., by dividing the data in smaller range blocks to accommodate the range variance of the SRC and higher order terms or by using a non-linear chirp scaling), the selection of a polychromatic kernel a la omega-k seems to be the most suited approach. As discussed in [2], an efficient approach to compute numerically the focussing kernel is

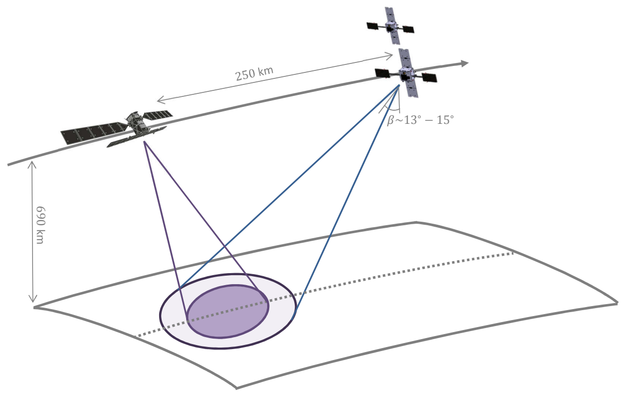

Fig. 1. Sketch of the STEREOID acquisition geometry with both receivers in front of the Sentinel-1 satellite. The processing-relevant bistatic squint angles are halved w.r.t. those shown in the plot.

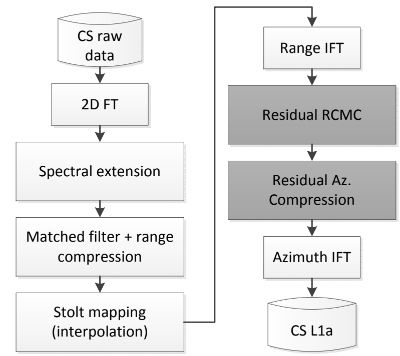

Fig. 2. Block diagram of the proposed numerical processing algorithm for large along-track bistatic baselines. CS stands for Companion Satellite.

by exploiting the singular value decomposition (SVD) of the two-dimensional spectrum of a set of reference point targets located at different range distances. Alternatively, a least-squares solution in order to simplify the processing steps is also possible in some cases, as also mentioned in [2]. Even though the numerical approach in [2] is presented in the frame of high resolution spaceborne monostatic SAR imaging, its extension to the bistatic case is straightforward. Figure 2 presents the block diagram of the proposed processing algorithm. The shaded blocks are optional and only required for the most challenging scenarios (e.g., very high resolution or forward looking). The first shaded block performs and additional interpolation in the range-Doppler domain (residual range cell migration correction block), while the second one performs a residual azimuth compression step. The spectral extension block might be required in order to consider the skew of the azimuth spectrum under squinted geometries if the system PRF is not large enough, as already pointed out in [6]. Fig. 3 shows the impulse response function of three targets after processing with the proposed numerical omega-k kernel, where it can be observed that the focusing is accurate for the complete imaged swath of $80\,\mathrm{km}$. The raw data were generated using a time-domain simulator for point-like targets. The acquisition geometry corresponds to the last Sentinel-1 sub-swath, where an azimuth resolution of $1\,\mathrm{m}$ and a chirp bandwidth of $50\,\mathrm{MHz}$ were simulated. Even if the azimuth resolution of the IW mode is just $20\,\mathrm{m}$, the reason to simulate one meter is to demonstrate the possibility of the kernel to process the complete Doppler span of the TOPS signal within a burst, which is about $5\,\mathrm{kHz}$. The processor has been implemented to have the option to focus the data in a beam-center geometry, which is advantageous for InSAR applications (see next section).

3. INSAR ASPECTS

3.1. InSAR Processing

Similar as with SAR image formation, interferometry becomes a challenge under high squinted scenarios, especially in terms of coregistration requirements. As is well known, the presence of an azimuth or a range coregistration error under squint can introduce large phase biases due to the presence of azimuth and phase ramps, respectively, in the impulse response function [7, 8]. The phase ramp in range can be completely removed if a beam-center geometry instead of a zero-Doppler one is used, and therefore is not considered in the following. The phase bias due to an azimuth coregistration error is given by $\varphi_{\mathrm{bias}}^{\mathrm{az}} = 2\pi \cdot f_{\mathrm{DC}} \cdot \Delta t$, where Δt represents the azimuth coregistration error in seconds and f_{DC} is the Doppler centroid. As mentioned before, in the STEREOID mission the Doppler centroid will be $-35\,\mathrm{kHz}$ in the worst case (near range). With these numbers, it turns out that a coregistration accuracy of $3\,\mathrm{mm}$ in azimuth is required in order to have a phase bias smaller than $5°$. In order to achieve such a stringent coregistration requirement we propose to use a geometric coregistration approach based on an external DEM and accurate orbit information. The required DEM accuracy will depend on the magnitude of the crossing orbit angle between image pairs, which depends on the selected orbital tube [9]. For the STEREOID mission, current available DEMs, e.g., SRTM or TanDEM-X, suffice to meet the required coregistration accuracy. Afterwards, only a constant coregistration error might remain, usually associated to the limited orbit knowledge. The residual coregistration error can be estimated by exploiting the ESD technique at the overlap areas between bursts, as conventionally done for the interferometric processing of TOPS data [10, 11].

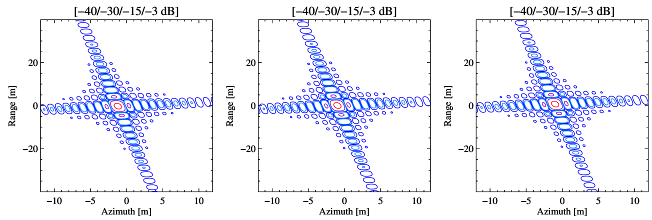

Fig. 3. Interpolated impulse response function in beam-center geometry of three simulated point targets after processing with the proposed numerical omega-k algorithm. Simulation corresponding to the last Sentinel-1 sub-swath scenario with a $1\ \mathrm{m}$ azimuth resolution and an along-track baseline of $250\ \mathrm{km}$, which results in an equivalent squint angle of $-6.5°$. Targets arranged from (left) near range to (right) far range.

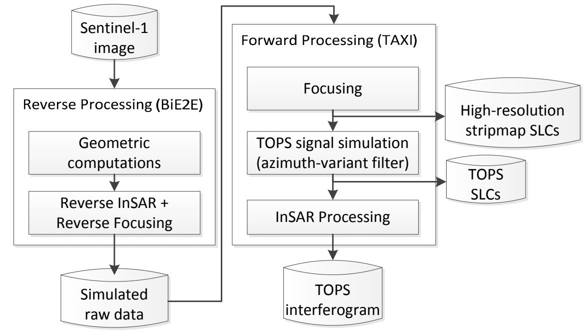

Fig. 4. Block diagram for the simulation and processing of an STEREOID pair using the Bistatic E2E simulator and the TAXI processor developed at DLR-HR.

3.2. Simulation Results

In order to perform the interferometric investigations, the bistatic end-to-end (BiE2E) simulator available at DLR-HR has been used [12]. The BiE2E performs a reverse processing in order to generate raw data from an existing reflectivity map, which in the present case is based on a Sentinel-1 image, using also its original acquisition geometry (orbit and timing). The simulation flow is sketched in Fig. 4. After ingesting the Sentinel-1 image (including timing and orbit information), several geometric computations are performed required to generate the high-squint bistatic images from the zero-Doppler geometry of the Sentinel-1 reflectivity image. These computations include the interferometric phase that will be injected to the slave image, as well as the offsets to bring the image to the slave geometry. The full resolution complex image is generated by injecting wide-band speckle (i.e., complex noise with a zero-mean Gaussian distribution) to the reflectivity image. The speckle signals for master and slave are correlated depending on the desired coherence to be simulated, in order to ensure the pair is interferometrically consistent. For validation purposes, a coherence equal to one for the complete scene has been simulated. The reverse processing follows, which includes the reverse InSAR, i.e., the insertion of interferometric phase and the interpolation to the slant-range plane of the slave image, and the reverse focusing in order to generate the raw data. Additional effects (instrument, environment) have been omitted in the current simulation. The generation of the raw data is achieved by using a reverse processor based on the algorithm presented in Section 2. Since the BiE2E has not been extended yet to simulate the TOPS mode, the raw data have been generated with a high azimuth resolution of $1\ \mathrm{m}$, similar as done in the previous section to validate the processing algorithm. Once the raw data are available, they have been processed with the suggested numerical kernel integrated in the experimental TanDEM-X Interferometric processor (TAXI) [13]. In order to simulate TOPS single-look complex images, the $1\ \mathrm{m}$ azimuth resolution stripmap images have been filtered and decimated by using an azimuth-variant Doppler filter, so that the Doppler spectral support of the azimuth signal is the same as for the Sentinel-1 IW mode. Note that several bursts are generated from the stripmap acquisition. Finally, the conventional TOPS interferometric processing chain integrated in TAXI (without any additional modification) has been used to compute the TOPS interferograms. Note that the complete processing chain (raw data focusing plus interferometric processing) is performed in beam-center geometry for the STEREOID case.

The main results are shown in Fig. 5. The image has a size of about $60\ \mathrm{km}$ in ground range and $76\ \mathrm{km}$ in azimuth and is composed of four Sentinel-1 bursts (each of $20\ \mathrm{km}$ length). The original Sentinel-1 data take is over Italy, close to Naples. The simulated along-track baseline is $250\ \mathrm{km}$ resulting in about $-35\ \mathrm{kHz}$ Doppler centroid. The spectral decorrelation due to sloped terrain can be observed, since note that no spectral filter was applied during the InSAR processing. An artificial along-track error of $1\ \mathrm{cm}$ was introduced in the slave orbit, which would result in a small azimuth phase ramp along the bursts if not corrected. However, the conventional TOPS InSAR chain exploiting ESD could estimate it with enough accuracy thanks to the large number of independent samples at the overlap areas. Consequently, no interferometric artifacts due to the high Doppler centroid are present. This result validates the proposed processing chain for the interferometric processing of high-squinted bistatic TOPS acquisitions.

4. SUMMARY

This contribution has presented some technical aspects related to the processing of SAR data in the frame of the STEREOID mission, candidate to ESA's Earth Explorer 10 mission. For the bistatic SAR image formation under high squints, an algorithm based on a numerical omega-k kernel has been suggested, which has been validated with point target simulations. On the other hand, the interferometric in-

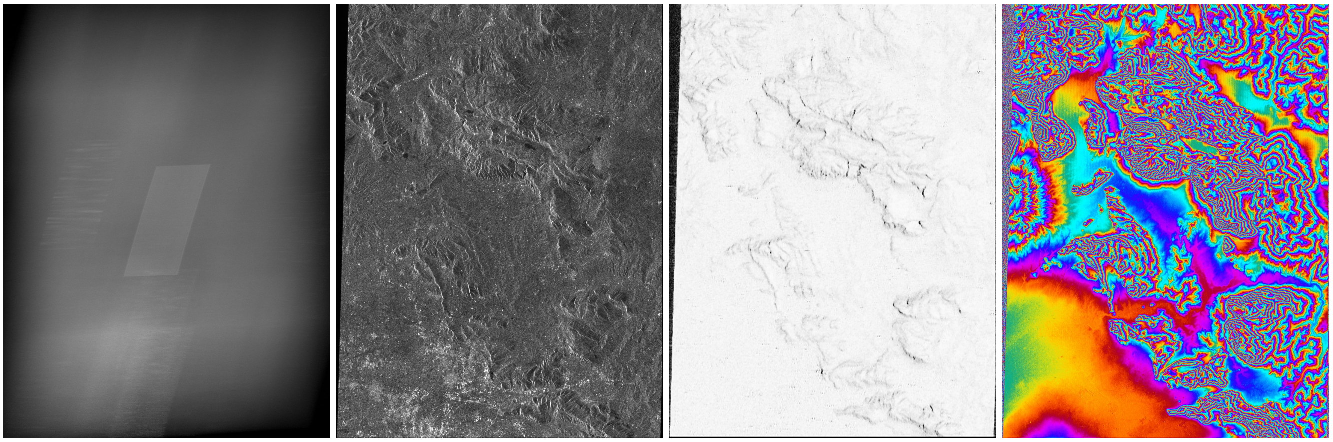

(a) Stripmap raw data (b) TOPS reflectivity image (c) TOPS interferometric coherence (d) TOPS interferometric phase

Fig. 5. Interferometric results obtained with the BiE2E and TAXI after simulating a TOPS acquisition with a bistatic along-track baseline of 250 km w.r.t. the Sentinel-1 satellite, corresponding to a Doppler centroid of about -35 kHz. The raw data on the left corresponds to the 1 m azimuth resolution stripmap acquisition. The coherence is scaled from zero (black) to one (white).

vestigations have been validated using the bistatic end-to-end chain available at DLR-HR. The final interferograms show no visible artifacts, hence validating the proposed InSAR processing strategy. These results confirm the possibility to efficiently process data acquired in the frame of the STEREOID mission.

Future steps include the extension of the bistatic E2E and TAXI with additional simulation and processing features, like the simulation of TOPS raw data, the digital beamforming in azimuth and in elevation, or the bistatic synchronization strategy.

5. REFERENCES

[1] I. G. Cumming and F. H. Wong, *Digital Processing of Synthetic Aperture Radar Data. Algorithms and Implementation*. Boston, London: Artech House, 2005.

[2] D. D'Aria and A. Monti Guarnieri, "High-resolution spaceborne SAR focusing by SVD-Stolt," *IEEE Geosci. Remote Sens. Lett.*, vol. 4, no. 4, pp. 639–643, Oct. 2007.

[3] P. Prats-Iraola, R. Scheiber, M. Rodriguez-Cassola *et al.*, "On the processing of very high-resolution spaceborne SAR data," *IEEE Trans. Geosci. Remote Sens.*, vol. 52, no. 10, pp. 6003–6016, Oct. 2014.

[4] I. Walterscheid, J. H. Ender, A. R. Brenner *et al.*, "Bistatic SAR processing and experiments," *Geoscience and Remote Sensing, IEEE Transactions on*, vol. 44, no. 10, pp. 2710–2717, 2006.

[5] R. Bamler, F. Meyer, and W. Liebhart, "Processing of bistatic SAR data from quasi-stationary configurations," *IEEE Trans. Geosci. Remote Sens.*, vol. 45, no. 11, pp. 3350–3358, Nov. 2007.

[6] G. W. Davidson and I. Cumming, "Signal properties of spaceborne squint-mode SAR," *IEEE Trans. Geosci. Remote Sens.*, vol. 35, no. 3, pp. 611–617, May 1997.

[7] M. Bara, R. Scheiber, A. Broquetas *et al.*, "Interferometric SAR signal analysis in the presence of squint," *IEEE Trans. Geosci. Remote Sens.*, vol. 38, no. 5, pp. 2164–2178, Sep. 2000.

[8] G. Fornaro, E. Sansosti, R. Lanari *et al.*, "Role of processing geometry in SAR raw data focusing," *IEEE Trans. Aerosp. Electron. Syst.*, vol. 38, no. 2, pp. 441–454, Apr. 2002.

[9] P. Prats-Iraola, M. Rodriguez-Cassola, F. De Zan *et al.*, "Role of the orbital tube in interferometric spaceborne SAR missions," *IEEE Geosci. Remote Sens. Lett.*, 2015, to be published.

[10] P. Prats, R. Scheiber, L. Marotti *et al.*, "TOPS interferometry with TerraSAR-X," *IEEE Trans. Geosci. Remote Sens.*, vol. 50, no. 8, pp. 3179–3188, Aug. 2012.

[11] N. Yague-Martinez, P. Prats-Iraola, F. R. Gonzalez *et al.*, "Interferometric processing of Sentinel-1 TOPS data," *IEEE Trans. Geosci. Remote Sens.*, vol. 54, no. 4, pp. 2220–2234, 2016.

[12] M. Rodriguez-Cassola, P. Prats-Iraola, M. Pinheiro *et al.*, "End-to-end level-0 data simulation tool for future spaceborne SAR missions," in *Proc. EUSAR*, Aachen, Germany, 2018.

[13] P. Prats, M. Rodriguez-Cassola, L. Marotti *et al.*, "TAXI: A versatile processing chain for experimental TanDEM-X product evaluation," in *Proc. IEEE International Geoscience and Remote Sensing Symposium (IGARSS'10)*, Honolulu, Hawai, USA, Jul. 25–30 2010.